

Supporting Information

Effective Adsorption of Pd(II), Pt(IV) and Au(III) by Zr-Cluster-Based Metal-Organic Frameworks from Strongly Acidic Solution

Shuo Lin, D. Harikishore Kumar Reddy, John Kwame Bediako, Myung-Hee Song, Wei Wei, Jeong-Ae Kim, and Yeoung-Sang Yun*

School of Chemical Engineering, Chonbuk National University, Jeonbuk 54896, Republic of Korea

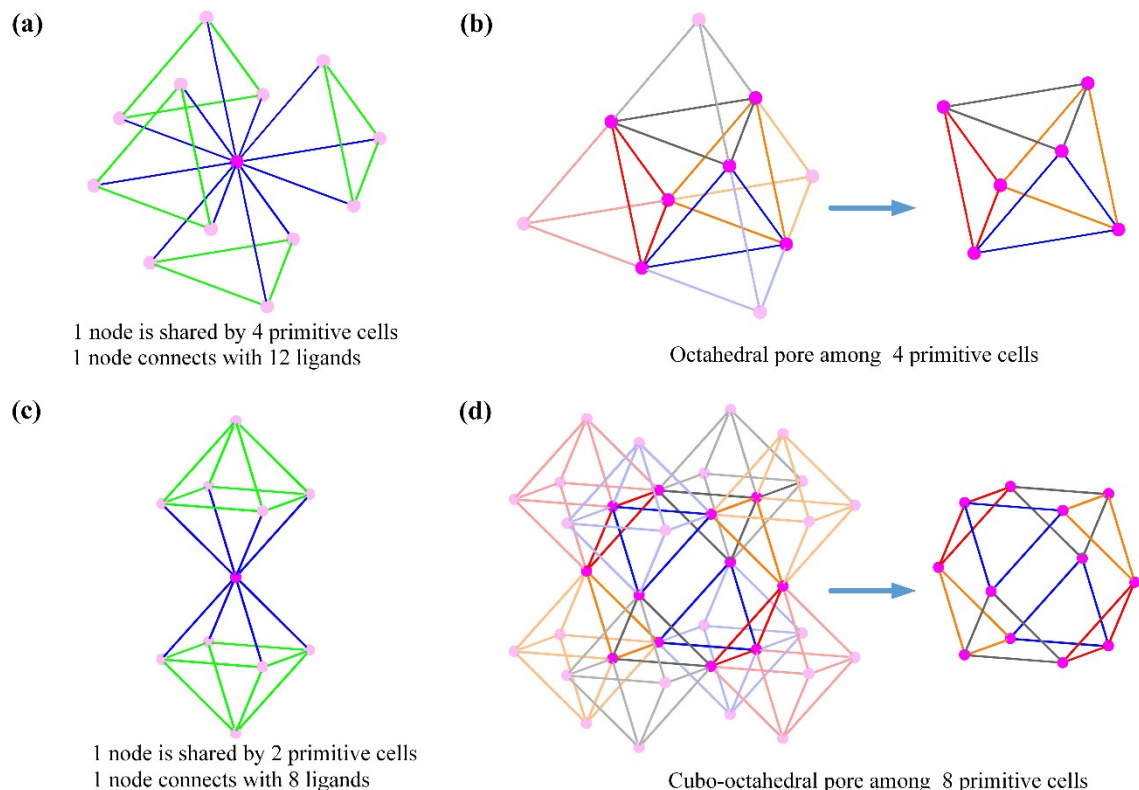


Fig. S1. Topological analysis of tetrahedral primitive cells (a, b) and octahedral primitive cell (c, d).

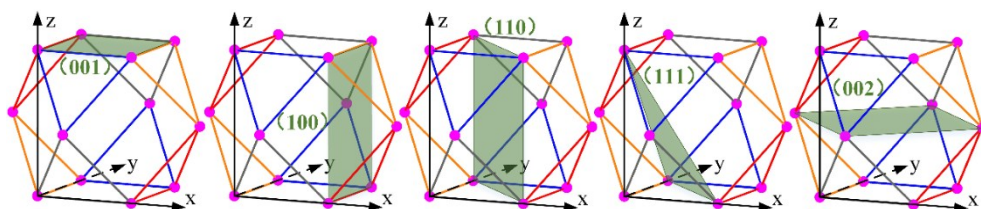


Fig. S2. Crystal face exponent (hkl) of cubo-octahedral unit cell.

Table S1. Lattice parameters of UiO-66 and UiO-66-NH₂ before and Pd(II), Pt(IV) and Au(III) adsorption. The experimental parameters were determined from powder X-ray diffraction and MDI Jade 6.5 (Materials Data Inc.).

MOFs	a=b (Å)	c (Å)	α (°)	β (°)	γ (°)
UiO-66	10.61	12.31	90	90	90
UiO-66-Pd	10.56	12.20	90	90	90
UiO-66-Pt	10.55	12.20	90	90	90
UiO-66-Au	10.52	12.10	90	90	90
UiO-66-NH₂	10.55	12.21	90	90	90
UiO-66-NH₂-Pd	10.54	12.20	90	90	90
UiO-66-NH₂-Pt	10.40	11.98	90	90	90
UiO-66-NH₂-Au	10.44	12.10	90	90	90

Table S2. Elemental analysis on UiO-66 and UiO-66-NH₂.

Complex (Atomic ratio)	% Zr	% Cl	% C	% N	% O
Observed UiO-66	7.62	1.93	52.50	0.0	37.99
Calculated for Zr₆O₄(OH)₄(BDC)₄(OH)_{2.5}Cl_{1.5}(EtOH)_{4.5}	7.55	1.89	51.57	0.0	38.99
Calculated for Zr₆O₄(OH)₄(BDC)₆Cl_{1.5}	6.86	1.71	54.86	0.0	36.57
Observed UiO-66-NH₂	6.86	1.77	47.80	4.64	38.92
Calculated for Zr₆O₄(OH)₄(BDC-NH₂)₄(OH)_{2.5}Cl_{1.5}(EtOH)₅(H₂O)_{2.5}	6.85	1.71	48.00	4.57	38.86
Calculated for Zr₆O₄(OH)₄(BDC-NH₂)₆Cl_{1.5}	6.42	1.60	51.34	6.42	34.22

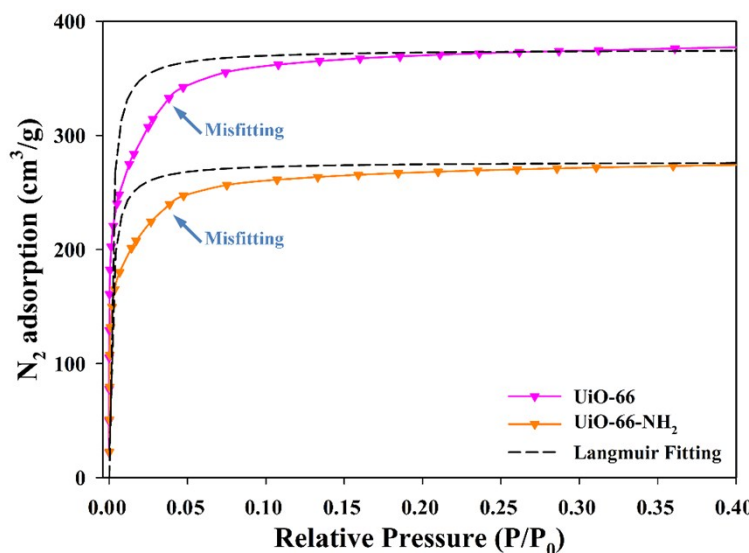


Fig. S3. N₂ isotherms of UiO-66 and UiO-66-NH₂ at 77 K. Solid line shows the observed data, and the dash line shows the Langmuir fitted data. (Only the data from 0 to 0.40 P/P₀ is shown)

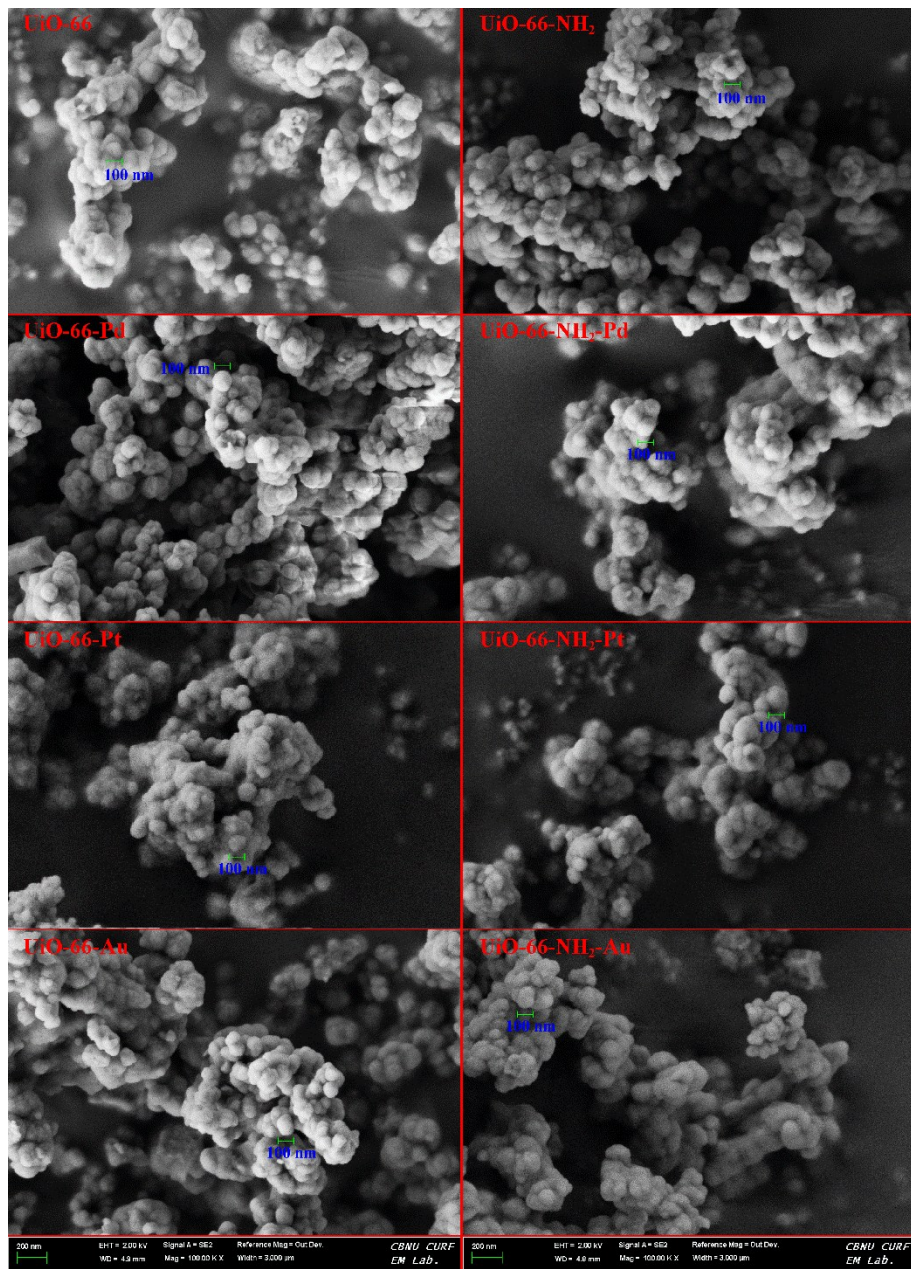
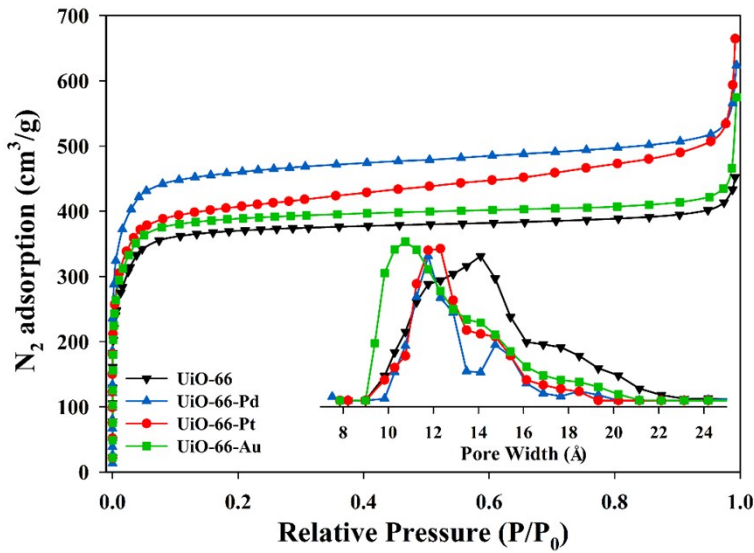


Fig. S4. FE-SEM images for UiO-66 and UiO-66-NH₂ respectively, upon the treatment with acidic Pd(II), Pt(IV) and Au(III) solutions (in 0.1 M HCl solution).

(a)



(b)

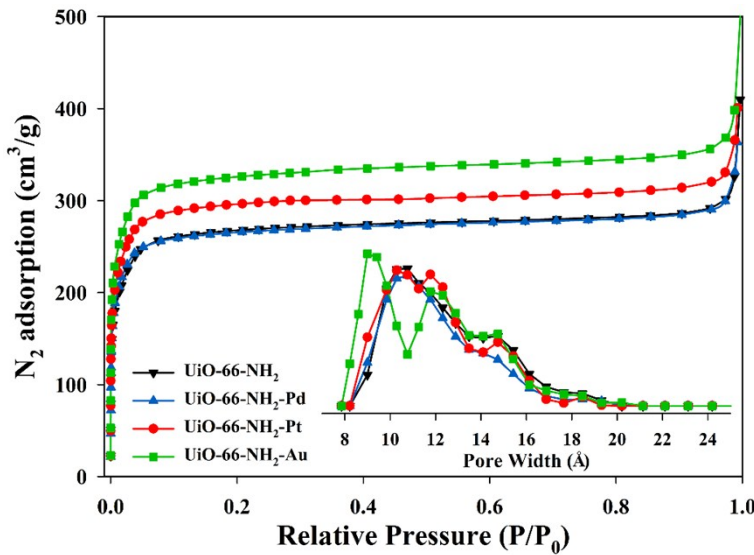


Fig. S5. N₂ isotherms of UiO-66 (a) and UiO-66-NH₂ (b) after immersion in Pd(II), Pt(IV) and Au(III) solutions (in 0.1 M HCl solution). Inlet shows pore size distributions as determined *via* DFT.

Table S3. N₂ uptake, BET surface area, total pore volume and pore width of UiO-66 and UiO-66-NH₂ before and after immersion in Pd(II), Pt(IV) and Au(III) solutions (in 0.1 M HCl solution).

MOFs	N ₂ uptake (cm ³ STP/g))	BET surface area (m ² /g)	Total pore volume (cm ³ /g)	Pore width (Å)
UiO-66	356	1551	0.686	12.9 and 16.1
UiO-66-Pd	422	1835	0.907	11.8 and 14.7
UiO-66-Pt	375	1634	0.967	11.8 and 14.7
UiO-66-Au	356	1550	0.793	10.8 and 14.1
UiO-66-NH ₂	245	1067	0.541	10.8 and 14.7
UiO-66-NH ₂ -Pd	243	1056	0.533	10.3 and 14.1
UiO-66-NH ₂ -Pt	280	1219	0.588	10.3 and 14.7
UiO-66-NH ₂ -Au	308	1340	0.660	9.4, 11.8 and 14.7

Table S4. Pd(II), Pt(IV) and Au(III) uptake amounts of various adsorbents including UiO-66 and UiO-66-NH₂ at preliminary adsorption period.

Adsorbent	Pd(II)			Pt(IV)			Au(III)		
	pH	Time (min)	Uptake (mg/g)	pH	Time (min)	Uptake (mg/g)	pH	Time (min)	Uptake (mg/g)
Glycine modified crosslinked chitosan resin ¹	2.0	25	9	2.0	25	10	2.0	25	8
L-lysine modified crosslinked chitosan resin ²	2.0	10	11	1.0	10	11	2.0	10	9
Graphene Oxide ³	6.0	10	15	6.0	10	33	6.0	60	66
Functionalized silica-gel ⁴	2.3	10	14	na	na	na	na	na	na
Chitosan/graphene oxide composites ⁵	3.0	60	63	na	na	na	na	na	na
Thiourea-modified chitosan microspheres ⁶	2.0	20	42	2.0	20	57	na	na	na
Collagen-Fiber-Immobilized Tannins ⁷	na	na	na	na	na	na	2.5	10	56
Phosphine sulphide-type chelating polymers ⁸	na	na	na	na	na	na	5.0	60	59
UiO-66 (This work)	1.0	3	17	1.0	3	47	1.0	3	42
	1.0	45	30	1.0	45	57	1.0	45	53
UiO-66-NH ₂ (This work)	1.0	3	50	1.0	3	49	1.0	3	55
	1.0	45	117	1.0	45	70	1.0	45	76

“na”: not available in the reference.

Table S5. Pd(II), Pt(IV) and Au(III) maximum uptake amounts of various adsorbents including UiO-66 and UiO-66-NH₂.

Adsorbent	Pd(II)		Pt(IV)		Au(III)	
	pH	Uptake (mg/g)	pH	Uptake (mg/g)	pH	Uptake (mg/g)
Glycine modified crosslinked chitosan resin ¹	2.0	120	2.0	122	2.0	170
L-lysine modified crosslinked chitosan resin ²	2.0	109	1.0	129	2.0	70
Graphene Oxide ³	6.0	81	6.0	71	6.0	108
Functionalized silica-gel ⁴	2.3	106	na	na	na	na
Chitosan/graphene oxide composites ⁵	3.0	217	na	na	na	na
Thiourea-modified chitosan microspheres ⁶	2.0	112	2.0	130	na	na
Collagen-Fiber-Immobilized Tannins ⁷	na	na	na	na	2.5	732
Phosphine sulphide-type chelating polymers ⁸	na	na	na	na	5.0	552
UiO-66 (This work)	1.0	120	1.0	166	1.0	280
UiO-66-NH ₂ (This work)	1.0	167	1.0	193	1.0	495

Table S6. Number of Pd, Pt and Au ions adsorbed per node in UiO-66 and UiO-66-NH₂.

MOFs	Items	Maximum adsorption per node			Actual adsorption per node		
		Pd(II)	Pt(IV)	Au(III)	Pd(II)	Pt(IV)	Au(III)
UiO-66	Uptake (mg/g)	120	166	280	96	153	235
	Uptake per Node	1.6	1.2	2.0	1.3	1.1	1.7
UiO-66-NH ₂	Uptake (mg/g)	167	193	495	188	201	438
	Uptake per Node	2.2	1.4	3.6	2.5	1.5	3.2

Table S7. Zeta potentials of various adsorbents including UiO-66 and UiO-66-NH₂.

Adsorbent	pH	Zeta potential (mV)	pH	Zeta potential (mV)	Target adsorbate
Activated carbon⁹	9	-67	7	-46	Methylene blue
Graphene¹⁰	10	-45	7	-35	Sb(II)
Graphene oxide nanocomposite¹¹	10	-40	7	-35	Cd(II)
Ceria nanoparticles supported on carbon nanotubes¹²	9	-37	7	-30	As(III)
Fe–Mn binary oxide¹³	3	+28	7	-5	Phosphate
Amino-functionalized nanoparticles¹⁴	3	+37	7	-25	Cr(VI), Pd(II) and Au(III)
NH₂-MCM-41¹⁵	2	+37	5	0	Au(III)
Fe–Al–Ce trimetal oxide¹⁶	5	+48	7	+40	Fluoride
UiO-66 (This work)	1	+35	7	+31	Pd(III), Pt(IV) and Au(III)
UiO-66-NH₂ (This work)	1	+43	7	+28	Pd(III), Pt(IV) and Au(III)

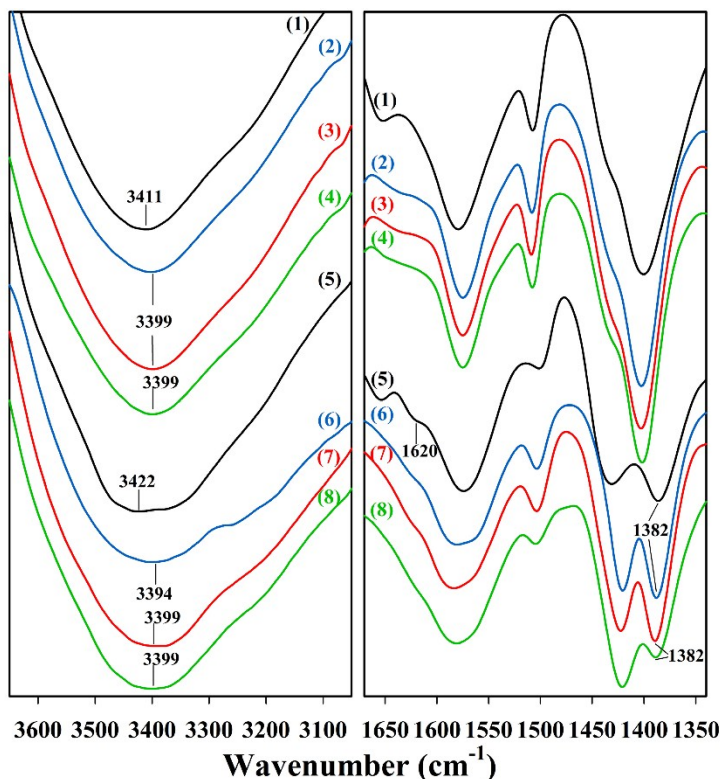


Fig. S6. FT-IR spectra from 3650 to 3050 cm⁻¹ and 1650 to 1350 cm⁻¹ of (1) pristine UiO-66 and after adsorption, (2) UiO-66-Pd, (3) UiO-66-Pt, (4) UiO-66-Au; (5) pristine UiO-66-NH₂ and after adsorption (6) UiO-66-NH₂-Pd, (7) UiO-66-NH₂-Pt and (8) UiO-66-NH₂-Au.

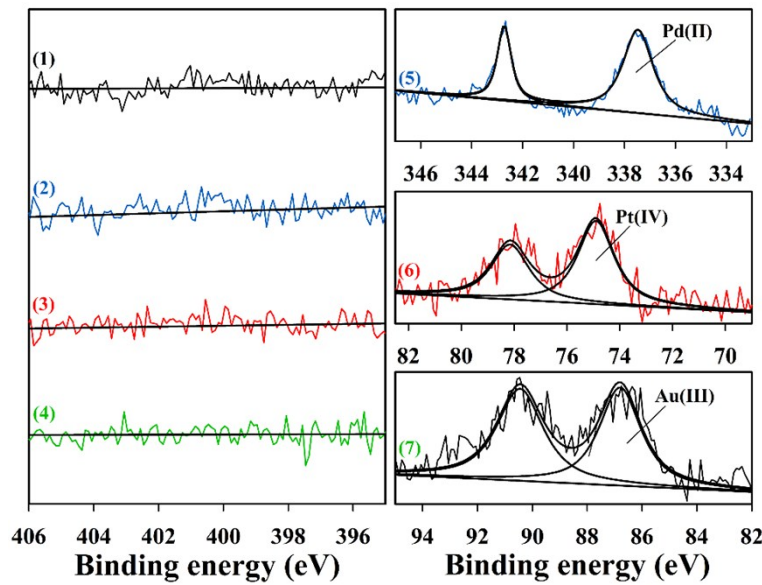


Fig. S7. XPS N 1s spectra of (1) pristine UiO-66 and after adsorption, (2) UiO-66-Pd, (3) UiO-66-Pt and (4) UiO-66-Au; XPS Pd 3d, Pt 4f and Au 4f spectra of UiO-66 after adsorption, (5) UiO-66-Pd, (6) UiO-66-Pt and (7) UiO-66-Au.

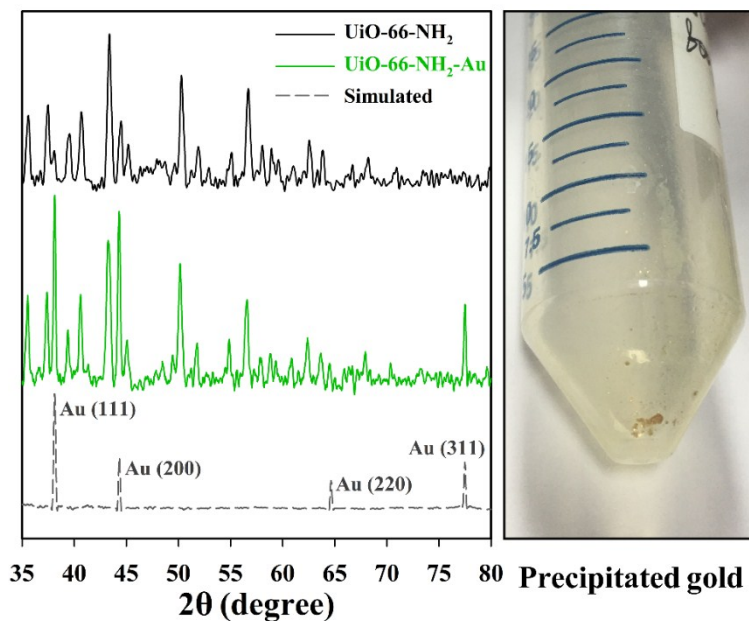


Fig. S8. XRD patterns (from 35 to 80 degree) of the pristine UiO-66-NH₂ and after Au adsorption (left). Image of falcon tube containing precipitated gold after adsorption in 800 and 1600 mg / L Au(III) solution (right).

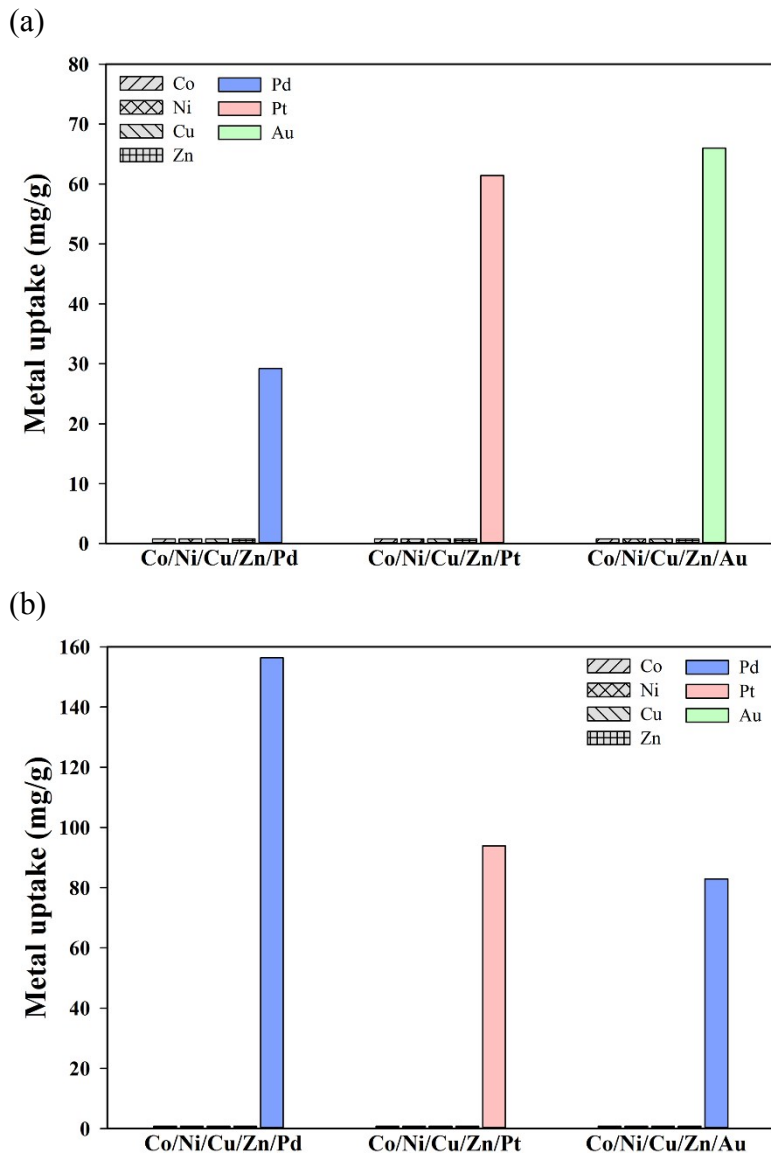


Fig. S9. Uptakes of various metals by UiO-66 (a) and UiO-66-NH₂ (b) mixed metal solutions containing Co(II), Ni(II), Cu(II), Zn(II), and precious metal ions with their respective concentrations of 100 mg / L. The mixed metal solutions were prepared by dissolving metal salts of CoCl₂·6H₂O, NiCl₂·6H₂O, CuCl₂ and ZnCl₂ as well as precious metal salts in 0.1 M HCl solution. In each case, 10 mg of MOF was exposed to mixed solutions at pH 1.0 for 24 h.

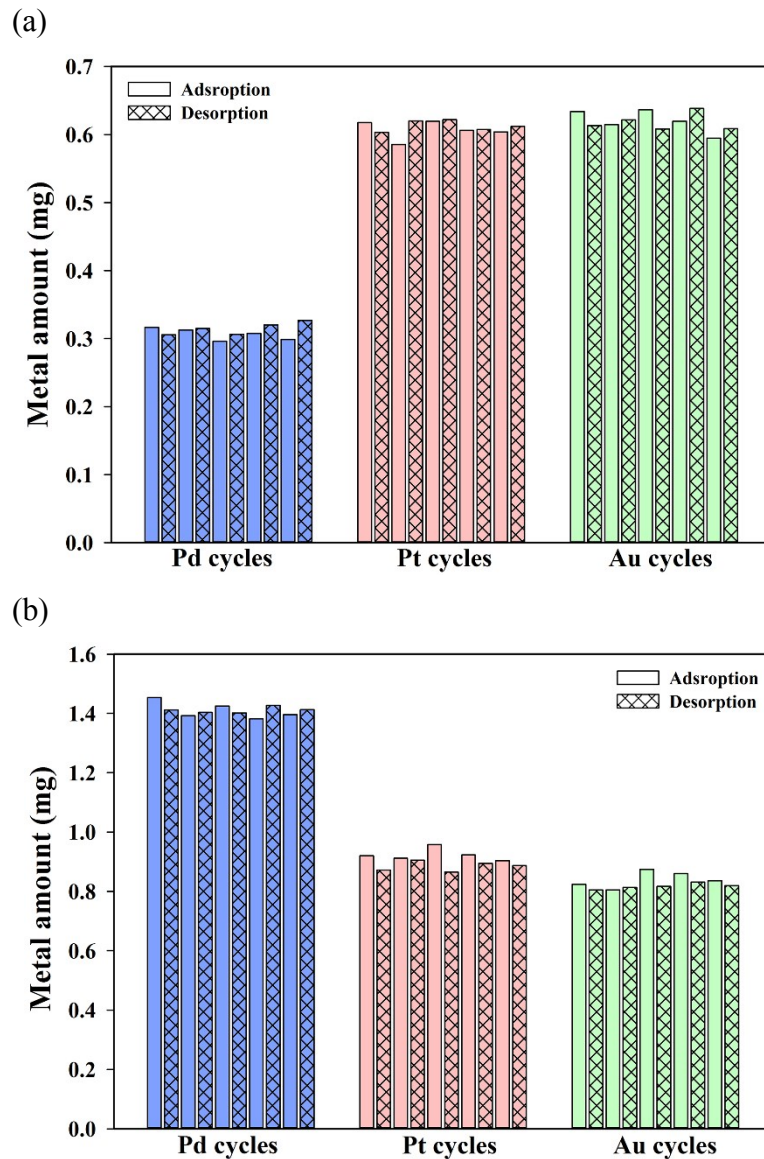


Fig. S10. Adsorption-desorption cycles of UiO-66 (a) and UiO-66-NH₂ (b) for Pd(II) (blue column), Pt(IV) (red column) and Au(III) (green column).

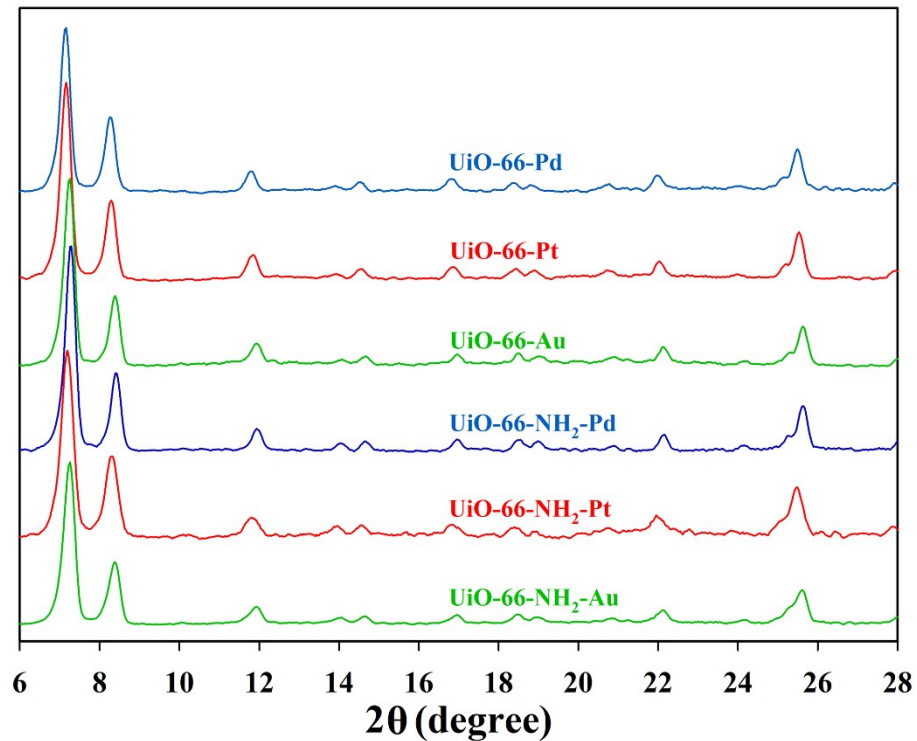


Fig. S11. PXRD patterns of UiO-66 and UiO-66-NH₂ after five cycles of adsorption-desorption.

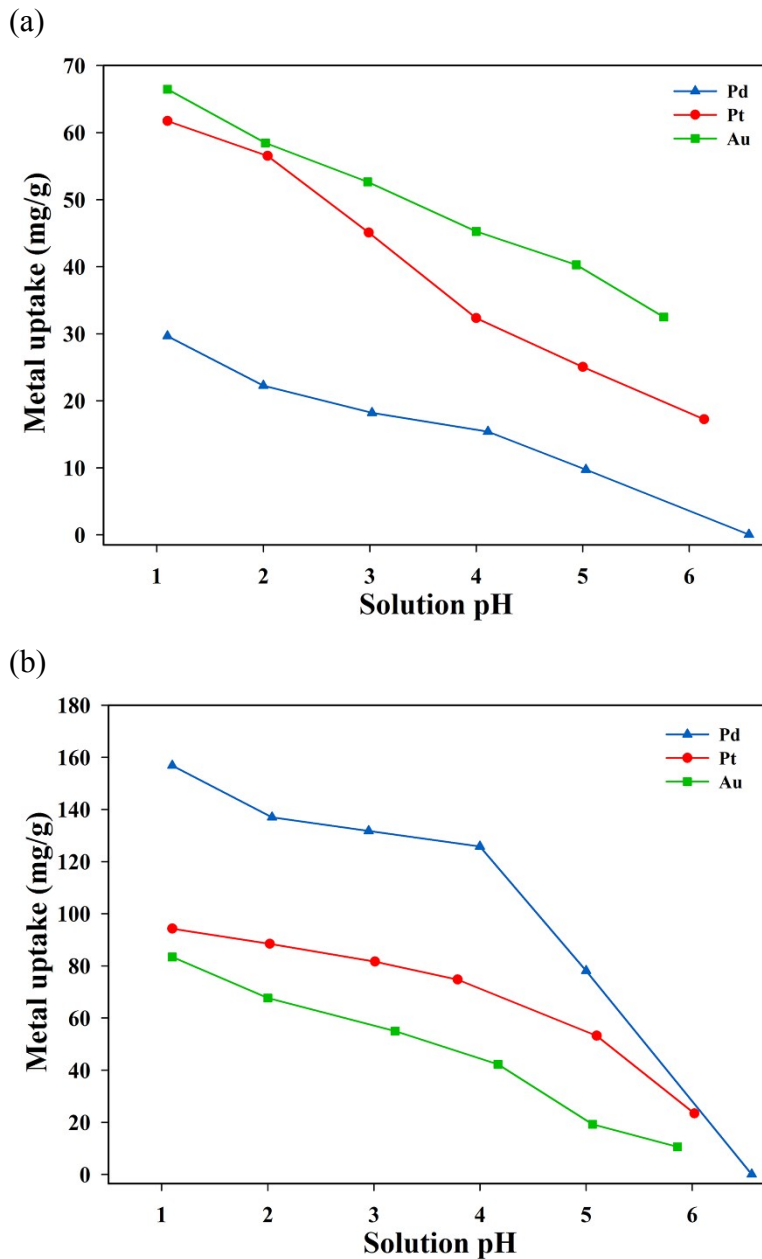


Fig. S12. The effect of solution pH on the adsorption of Pd(II), Pt(IV) and Au(III) onto UiO-66 (a) and UiO-66-NH₂ (b). In each case, 10 mg of MOF was exposed to 100 mg / L Pd(II), Pt(IV) and Au(III).

As seen in the figure, all the uptakes of Pd(II), Pt(IV) and Au(III) onto the UiO-66 and UiO-66-NH₂ generally decreased with the increasing of solution pH. These were due to the positively charged functional groups in the UiO-66 and UiO-66-NH₂ and the species of Pd(II), Pt(IV) and Au(III) significantly influenced by the solution pH. As the solution pH increased, the charge of the functional groups would tend to neutral. In addition, the PdCl_4^{2-} , PtCl_6^{2-} and AuCl_4^- species of Pd(II), Pt(IV) and Au(III) would turn to PdO , PtO_2 and Au(OH)_3 , respectively (the fraction of each species of metals was simulated by Medusa software). This is likely the reason why the adsorption capacity decreased with the increasing of the solution pH.

References:

- 1 A. Ramesh, H. Hasegawa, W. Sugimoto, T. Maki and K. Ueda, *Bioresour. Technol.*, 2008, **99**, 3801-3809.
- 2 K. Fujiwara, A. Ramesh, T. Maki, H. Hasegawa and K. Ueda, *J. Hazard. Mater.*, 2007, **146**, 39-50.
- 3 L. Liu, S. X. Liu, Q. P. Zhang, C. Li, C. L. Bao, X. T. Liu and P. F. Xiao, *J. Chem. Eng. Data.*, 2013, **58**, 209-216.
- 4 R. J. Qu, Y. Z. Ni, J. H. Liu, C. M. Sun, Y. Zhang, H. Chen and C. N. Ji, *React. Funct. Polym.*, 2008, **68**, 1272-1280.
- 5 L. Liu, C. Li, C. Bao, Q. Jia, P. Xiao, X. Liu and Q. Zhang, *Talanta*, 2012, **93**, 350-357.
- 6 L. Zhou, J. Liu and Z. Liu, *J. Hazard. Mater.*, 2009, **172**, 439-446.
- 7 X. Liao, M. Zhang and B. Shi, *Ind. Eng. Chem. Res.*, 2004, **43**, 2222-2227.
- 8 J. M. Sánchez, M. Hidalgo and V. Salvadó, *React. Funct. Polym.*, 2001, **46**, 283-291.
- 9 Y. H. Li, Q. J. Du, T. H. Liu, X. J. Peng, J. J. Wang, J. K. Sun, Y. H. Wang, S. L. Wu, Z. H. Wang, Y. Z. Xia and L. H. Xia, *Chem. Eng. Res. Des.*, 2013, **91**, 361-368.
- 10 Y. Q. Leng, W. L. Guo, S. N. Su, C. L. Yi and L. T. Xing, *Chem. Eng. J.*, 2012, **211**, 406-411.
- 11 J. H. Deng, X. R. Zhang, G. M. Zeng, J. L. Gong, Q. Y. Niu and J. Liang, *Chem. Eng. J.*, 2013, **226**, 189-200.
- 12 X. Peng, Z. Luan, J. Ding, Z. Di, Y. Li and B. Tian, *Mater. Lett.*, 2005, **59**, 399-403.
- 13 G. Zhang, H. Liu, R. Liu and J. Qu, *J. Colloid Interface Sci.*, 2009, **335**, 168-174.
- 14 S. H. Huang and D. H. Chen, *J. Hazard. Mater.*, 2009, **163**, 174-179.
- 15 K. F. Lam, C. M. Fong, K. L. Yeung and G. McKay, *Chem. Eng. J.*, 2008, **145**, 185-195.
- 16 X. Wu, Y. Zhang, X. Dou and M. Yang, *Chemosphere*, 2007, **69**, 1758-1764.